Hindawi
International Journal of Antennas and Propagation
Volume 2023, Article ID 6645672, 10 pages
https://doi.org/10.1155/2023/6645672

Research Article

A Ku Wideband Circularly Polarized Microstrip Antenna Array with Low Profile Crossed-Dipole Element

Haipeng Liu,[1,2] **Yunhua Zhang**,[1,2] **and Xiaowen Zhao**[1,2]

[1]*CAS Key Laboratory of Microwave Remote Sensing, National Space Science Center (NSSC), Chinese Academy of Sciences, Beijing 100190, China*
[2]*University of Chinese Academy of Sciences, Beijing 100049, China*

Correspondence should be addressed to Yunhua Zhang; zhangyunhua@mirslab.cn

Received 22 February 2023; Revised 26 April 2023; Accepted 8 May 2023; Published 19 May 2023

Academic Editor: Ding-Bing Lin

This paper presents a novel Ku wideband circularly polarized (CP) antenna array composed of crossed-dipole element (CDE) and fed through sequential rotation (SR) feeding technique. Unlike the traditional CP-CDE fed by coaxial cable that usually works at low frequencies, the proposed CDE consists of two orthogonal heart-shaped patch dipoles that can work at frequencies as high as Ku-band, at the same time achieving a larger bandwidth. A feeding structure is proposed without welding, so potential errors in the antenna assembly process can be mitigated. A 2×2 CP antenna array with wideband SR feeding network is designed based on the CDE to further expand the axial ratio (AR) bandwidth. The designed antenna array is fabricated using the multilayer printed circuit board (PCB) technology and measured in anechoic chamber using the planar near-field measurement facility. The measured results show that −10 dB impedance bandwidth of 44% (11.6–18.15 GHz) along with 3 dB AR bandwidth of 38.7% (12–17.65 GHz) and 3 dB gain bandwidth of 34.6% (12.2–17.3 GHz) as well as 11.02 dBic peak gain have been achieved while maintaining a lower profile.

1. Introduction

Circularly polarized (CP) antennas have many advantages compared with linear polarization (LP) antennas in mitigating multipath interference, reducing Faraday rotation effects, and suppressing polarization mismatch. Therefore, they are widely used in satellite communication systems and remote sensing [1–4]. Besides, the antenna array can achieve higher gain with narrower beamwidth to compensate the spatial attenuation for long-distance communication [5, 6].

Generally, a wideband CP antenna array highly depends on the wideband CP element. However, the design of CP elements with wide axial ratio (AR) bandwidth is usually difficult [7–10]. Another way to design a wideband CP antenna array is by using a sequential rotation (SR) technique based on LP or CP elements with unique angular and phase arrangements [11–14]. Up to now, many kinds of wideband CP arrays have been proposed with various sequential rotation (SR) feeding networks, such as series-feeding networks [11], corporate-feeding networks [15–19], and series-parallel feeding networks [20–23]. Despite these efforts, the achieved CP bandwidths have not exceeded 29% due to limitations in the bandwidth of the SR feeding network, or narrow bandwidth in the elements themselves. On the other hand, crossed-dipole antenna has been widely studied in recent years due to their wideband radiation performances, compact size, and ease of fabrication [24–29]. In [30], a wideband CP crossed-dipole antenna with parasitic elements was designed, where an AR bandwidth of 90.9% (2.2–6.4 GHz) has been achieved. However, it has a high profile ($0.4\lambda_0$), which is not suitable for space-constrained applications. Although the profile of the crossed-dipole has been reduced to $0.14\lambda_0$ with an AR bandwidth of 111.8% (1.75–6.19 GHz) in [31], the coaxial cable feeding structure of those antennas is not suitable for high-frequency applications since the assembly of the coaxial cable feeding structure is very challenging for avoiding the influence of solder joints on the radiation, which is especially serious at high frequencies. That is why the most reported CP

crossed-dipole antennas work at low frequencies. Therefore, changing the feeding structure is an effective way for crossed-dipole antennas for high-frequency applications. For instance, a CP magneto-electric dipole antenna was presented in [32] for K-band and Ka-band applications, which is fed through a modified cross-slot on the ground plane. In [33], a CP crossed-dipole antenna fed by metallic via-holes was designed for Ka-band application, and the reported bandwidth is just about 15.7%.

In this paper, a Ku wideband CP microstrip antenna array with low profile crossed-dipole element is proposed. The designed heart-shaped patch can effectively improve impedance matching by reducing edge reflections, and thus broadband crossed-dipole element (CDE) can be realized. In the design, a novel metal via feeding structure inspired by SIW is proposed to overcome the problem of the coaxial cable feeding structure adopted by conventional CDE working at high frequencies. The proposed feeding structure not only can be easily integrated into the antenna without solder joints using PCB technology, but also can avoid the potential errors during the assembly process of the antenna. Meanwhile, a wideband SR feeding network adapted to four CDEs is designed by cascading the Wilkinson power divider and the Schiffman phase shifter, which helps for realizing broadband CP array.

2. Antenna Element Design and Analysis

2.1. Structure of the Antenna Element. Figure 1 presents the structure of the proposed CDE with dimensions given. As can be seen, three substrates are used, and all of them are F4BM220 with dielectric constant of 2.2 and loss tangent of 0.001, and they are connected by bonding film with dielectric constant of 2.5 and thickness of 0.1 mm. Substrates I and III have the same thickness of 0.254 mm, while substrate II has a thickness of 1.587 mm. Two dipoles with a pair of heart-shaped patches are placed orthogonally and etched on the two top surfaces of substrates. The adjacent patches on the same surface are connected by a vacant-quarter-printed ring with a circumference of about $\lambda g/4$. The optimized parameters of the CDE are summarized in Table 1.

A novel feeding structure is proposed as inspired by substrate integrated waveguide (SIW) as shown in Figure 1(c). There are six blind vias (BVs) enclosed in a circle in substrate II, which are used to connect the patches at the top surface of the substrate II to the middle ground. A metal ring with a width of W_d acts as the pad of BVs and is placed above the BVs. Meanwhile, the microstrip line at the bottom of substrate III is connected to the patches on the top surface of substrate I by the through via (TV). The TV and the BVs act as the inner and the outer conductor of coaxial cable, respectively. According to the coaxial impedance formula [34], the dimensions of d_{out} and d_{in} are related to the characteristic impedance Z_0 of the coaxial cable as

$$Z_0 = \frac{1}{2\pi}\sqrt{\frac{\mu}{\varepsilon}}\ln\frac{d_{\text{out}}}{d_{\text{in}}}, \tag{1}$$

where d_{out} represents the diameter of the circle formed by the BVs and d_{in} represents the diameter of the TV.

2.2. Feeding Structure. Most of the reported CP single-feed crossed-dipole antennas operate at low frequencies since the coaxial cable feeding structure is not suitable for high frequencies [29]. At high frequencies, the influence of solder joints of the coaxial cable on the radiation cannot be ignored. In addition, the structure of the coaxial cable brings a considerable challenge to the assembly of the antenna due to welding requirements. In this subsection, a novel feed structure is proposed without solder joints to overcome aforementioned problems, and its principle is illustrated.

Figure 2 shows the electromagnetic field distributions of the proposed feeding structure and the usually used coaxial cable, as can be seen from which, the strength of the electromagnetic field is concentrated within the region enclosed by the BVs, as same as coaxial cable. However, discrete BVs may lead to discontinuities in the H-plane of the TEM wave, thus leading to radiation leakage if not properly designed. A transmission structure in Figure 3 is simulated to show the effect of the numbers and diameters of BVs on transmission performances. The variations of transmission performance corresponding to different numbers of the BVs are plotted in Figure 4. As can be seen that as the number of the BVs increases, the transmission performance of the proposed feeding structure approaches to those of coaxial cable, and the radiation leakage is correspondingly reduced. When the number of BVs is greater than 6, the insertion loss caused by the proposed feeding structure is close to that of the coaxial cable structure; it is to say that the spurious radiation has already been greatly reduced. However, it should be stressed more than 6 BVs, which does not bring about significant improvement in transmission performance but increases the complexity of production.

Figure 5 shows the effect of the diameter of the BVs on the transmission performance, from which one can see that the diameter of the BVs has a significant impact on transmission performance. This is because varying diameters of the BVs cause a perturbation in the electromagnetic field distributions, and when they all have the same diameter, the obtained electromagnetic distribution is similar to that of coaxial cable.

2.3. Performance Simulation and Design Process. To demonstrate the advantages of the proposed radiating patch, the cross dipole with bow-tie patch [25] is compared in the following. Figure 6 presents the geometries of the proposed CDE and that of [25], and these two CDEs have the same dimensions but different shapes of edges. Figure 7 presents the simulated $|S_{11}|$ and AR of our CDE and that of [25] over frequencies, as can be seen that their AR bandwidths are almost the same, while their impedance bandwidths are quite different; ours is obviously better because the edge reflection is reduced benefitting from the heart-shape. Finally, the impedance bandwidth and the AR bandwidth of the proposed CDE achieve 40% and 5.8%, respectively. Here, the impedance bandwidth achieves the broadband performance, which is a good precondition for achieving a wider 3 dB gain bandwidth of the array by adopting the SR technique, ultimately achieving the overall wideband CP performance of the array.

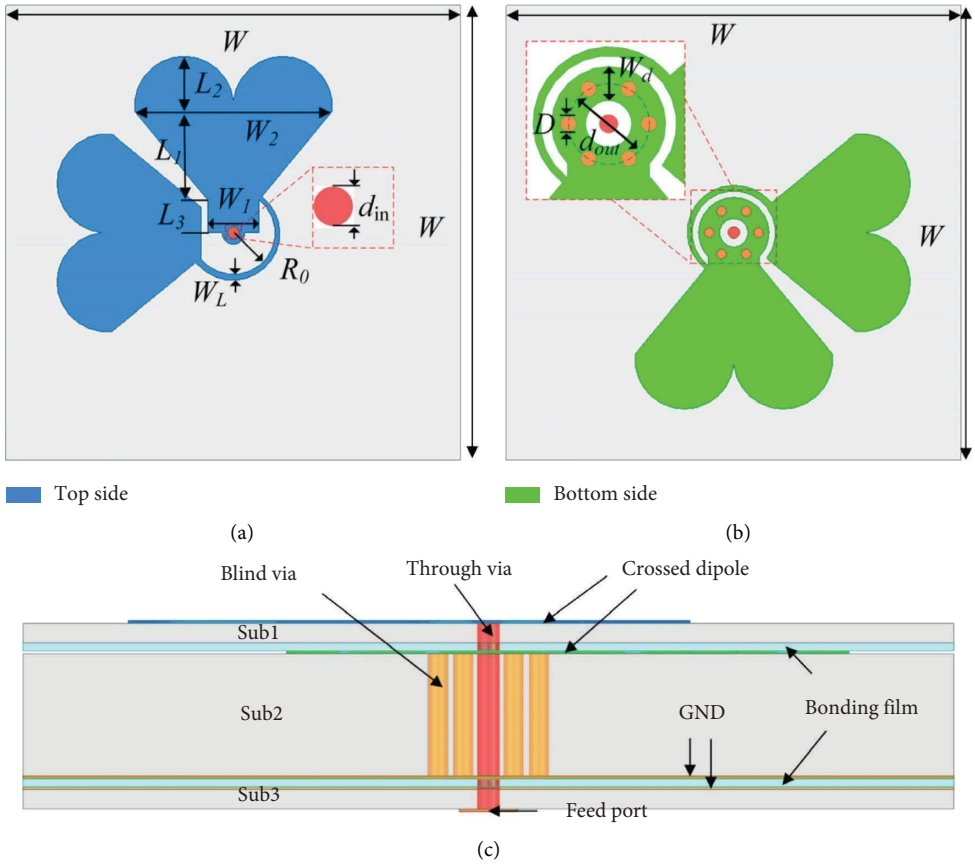

Figure 1: Structure of the proposed wideband CP crossed-dipole antenna. (a) Top view. (b) Bottom view. (c) Front view.

Table 1: Dimensions of the antenna element (unit: mm).

Parameter	Value
W	25
W_1	1.33
W_2	5.7
R_0	1.1
W_L	0.1
d_{out}	1.3
W_d	0.3
d_{in}	0.35
L_1	2.35
L_2	1.45
L_3	0.85
D	0.35

The design procedure for the proposed antenna is given as follows:

(1) To design a CP crossed-dipole antenna based on three substrates: The radiating patch of the antenna was designed using a pair of simple bow-tie patches on both surfaces of the top substrate. The bow-tie patches resonated at half the designed wavelength. The design principles and mechanism of the bow-tie patches are detailed in [25].

(2) To design the shape of the radiating patch by introducing circular arc at the edges of the patch to improve the impedance performance of the antenna.

(3) To design the metal via feeding structure with its dimensions calculated according to equation (1).

(4) To adjust the patch length (L_S) and the width (W_L) of the phase-shift ring to meet the designed working frequency band, adjust L_1 and W_2 of the patch to make the two resonate frequencies fall within the working frequency band, and adjust W_1 to improve the impedance matching within the working frequency band.

3. CP Antenna Array

A wideband 2×2 CP array with four CDEs is designed using the SR feeding network. The CP bandwidth of the array can be further enhanced by exciting the four CDEs with the same magnitude but a 90° phase difference in between. The configuration of the array is presented in Figure 8(a), where the CDEs are placed in turn by rotating 90°, and the adjoining distance is $0.625\lambda_0$ (λ_0 is free-space wavelength at 15 GHz).

As shown in Figure 8(b), the feeding network is printed on the bottom surface of substrate III, which includes a Wilkinson power divider, a Schiffman 180° phase shifter, and two Schiffman 90° phase shifters [35, 36]. Figure 9(a) shows the equivalent circuit of the feeding network, and Figure 9(b) presents the simulated results of S-parameters, as it is shown that the variation of

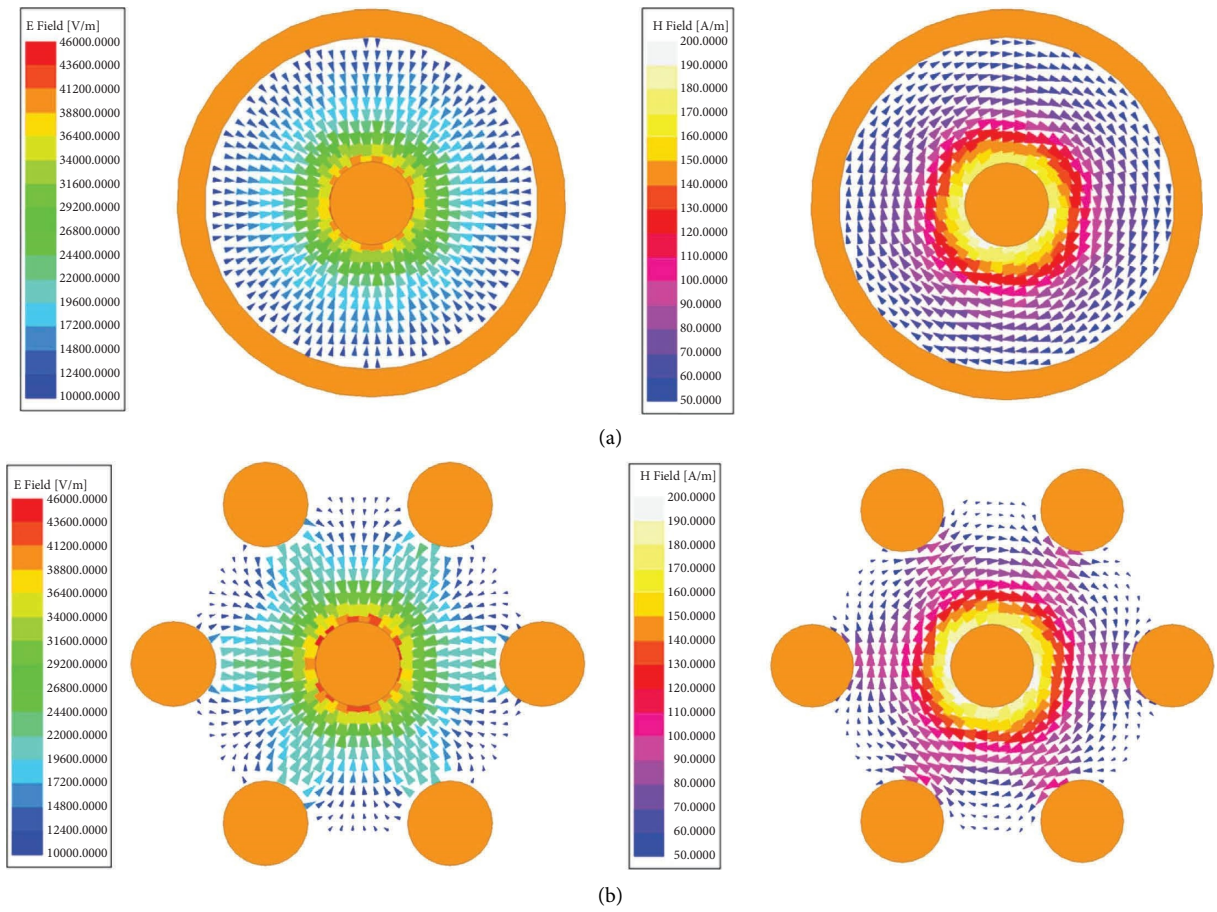

Figure 2: Electromagnetic field distribution of TEM wave. (a) Coaxial cable. (b) Proposed structure.

the output power between different ports is less than 0.5 dB, and the phase difference between two adjacent ports is less than 5°. The results indicate that the designed feeding network lays a good foundation for achieving a wideband CP array.

4. Experimental Results and Discussion

A 2 × 2 wideband CP antenna array is fabricated by using multilayer-printed circuit board technology, as shown in Figure 10(a); the three-dimensional sizes of which are 38 mm × 34 mm × 2.38 mm. Figure 10(b) gives the photo taken during the measurement. The fabricated array was measured in anechoic chamber by using the gain-comparison method, and the facility is the NSI 2000 planar near-field measurement system, where a standard horn antenna of LP is used as the reference antenna, whose gain has been accurately known, and the probe is also of LP. The measured gain can be calculated by [37]

$$G_{\mathrm{AUT}} = G_{\mathrm{STD}} - \Delta G + 20\log_{10}\left[0.5\left(1 + 10^{-(AR/20)}\right)\right] + 3, \quad (2)$$

where G_{AUT} is the gain of the array, G_{STD} is the gain of the used standard LP horn, ΔG is the received power difference between the standard LP horn and the array, and AR is the axial ratio of the array.

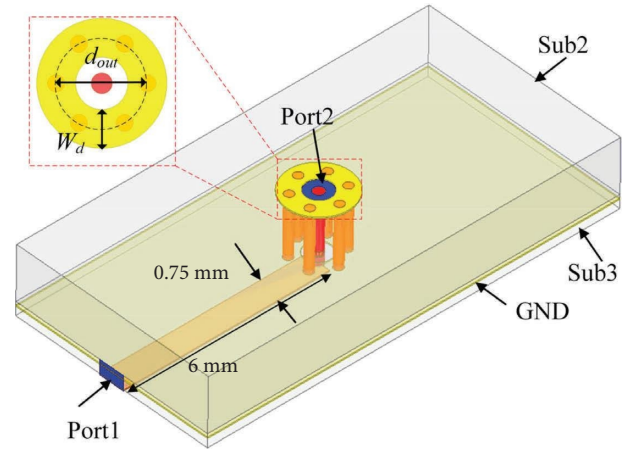

Figure 3: Configuration of the transmission structure.

The simulated and measured $|S_{11}|$ of the array are plotted in Figure 11(a) with good agreement. The measured impedance bandwidth with $|S_{11}| < -10$ dB is about 44% within 11.6–18.15 GHz, which is slightly less than the simulated result of 46.5%. Figure 11(b) depicts the measured and simulated ARs along with the gains at broadside direction. As can be seen, the simulated and measured 3 dB AR bandwidths are over 38.9% and 38.7%, respectively, within

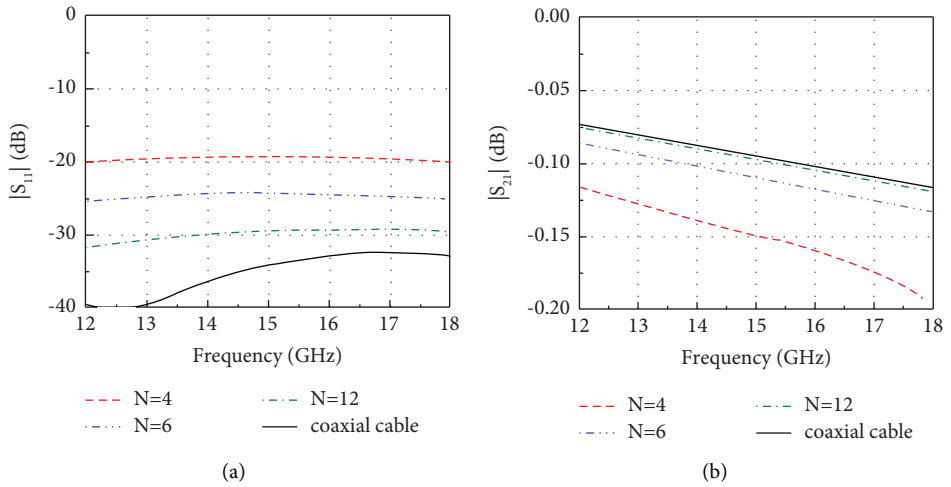

Figure 4: Transmission performance of the metal via structure versus the number of BVHs. (a) $|S_{11}|$. (b) $|S_{21}|$.

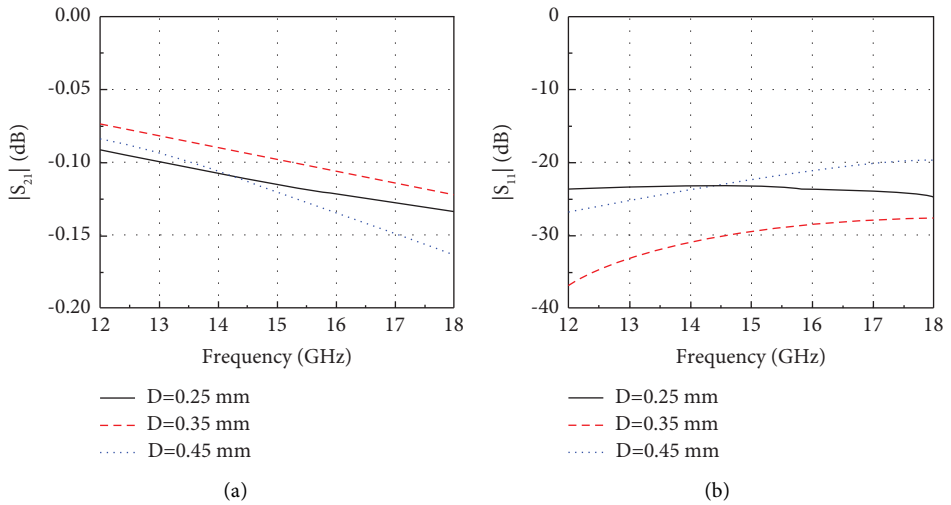

Figure 5: Transmission performance of the metal via structure versus the diameter of the BVHs. (a) $|S_{11}|$. (b) $|S_{21}|$.

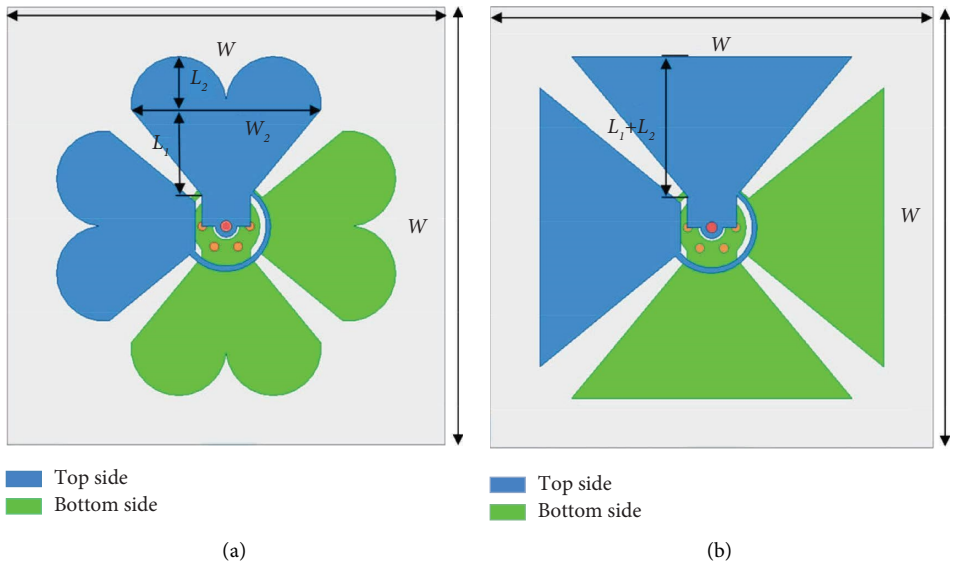

Figure 6: Structure of the (a) proposed element and (b) reference element [25].

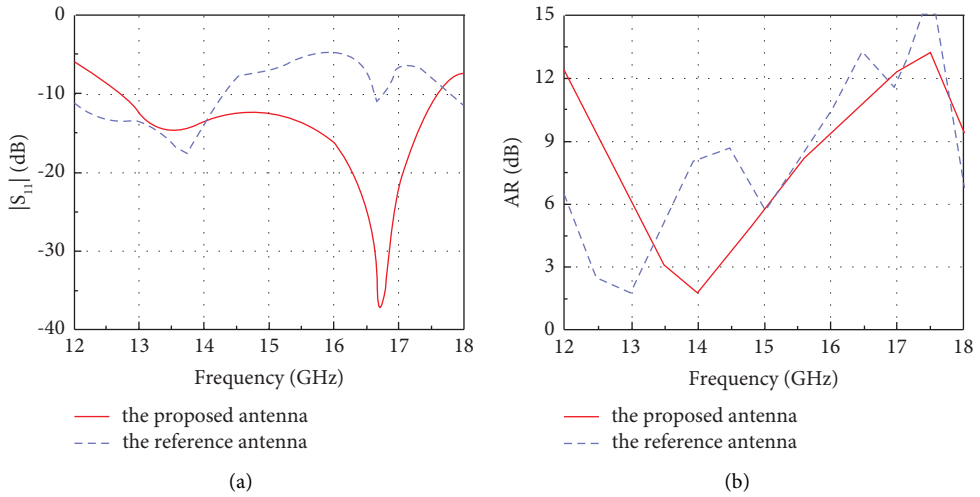

Figure 7: (a) $|S_{11}|$ and (b) AR simulations for Figure 6 in frequency range of 12–18 GHz.

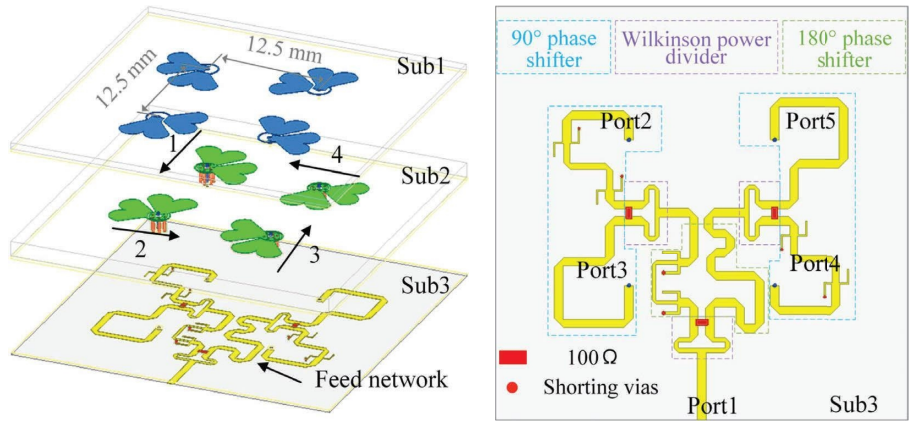

Figure 8: Proposed 2 × 2 antenna array. (a) Layout. (b) Feeding network.

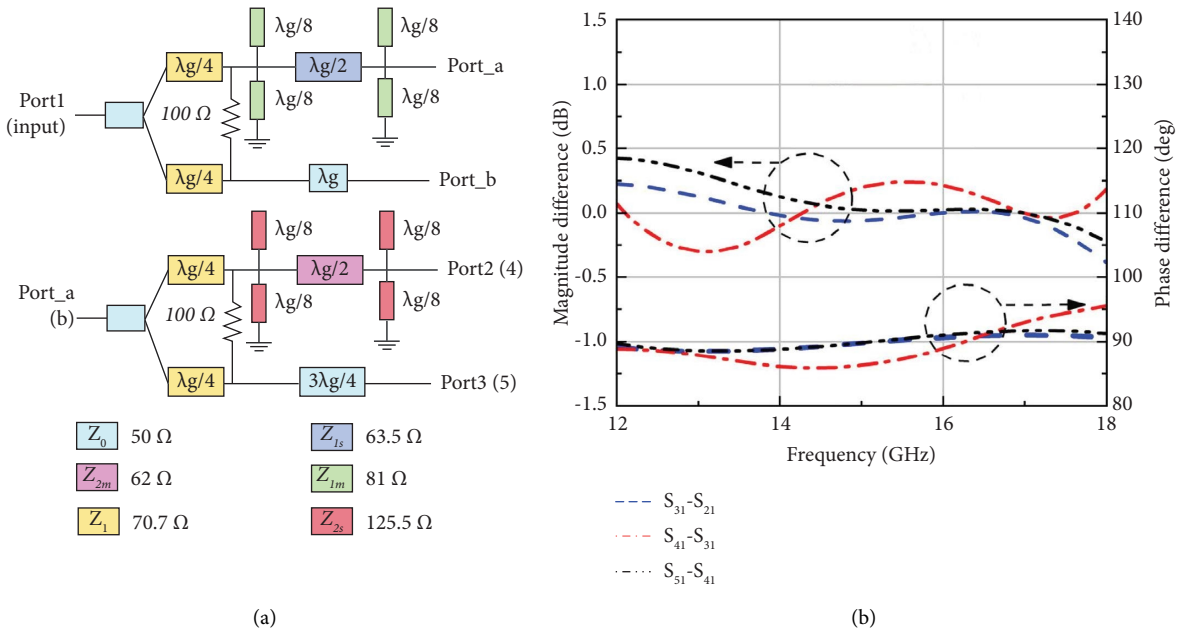

Figure 9: Wideband feeding network. (a) Equivalent circuit. Microstrip line width: w (Z_0) = 0.71 mm; w (Z_1) = 0.37 mm; w (Z_{1m}) = 0.3 mm; w (Z_{1s}) = 0.2 mm; w (Z_{2m}) = 0.53 mm; w (Z_{2s}) = 0.11 mm. (b) Transmission performance.

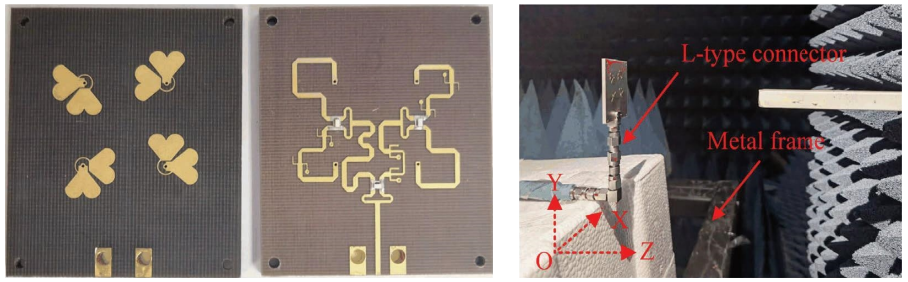

(a) (b)

Figure 10: Prototype of the array. (a) Top and bottom view. (b) Testing the array in microwave anechoic chamber.

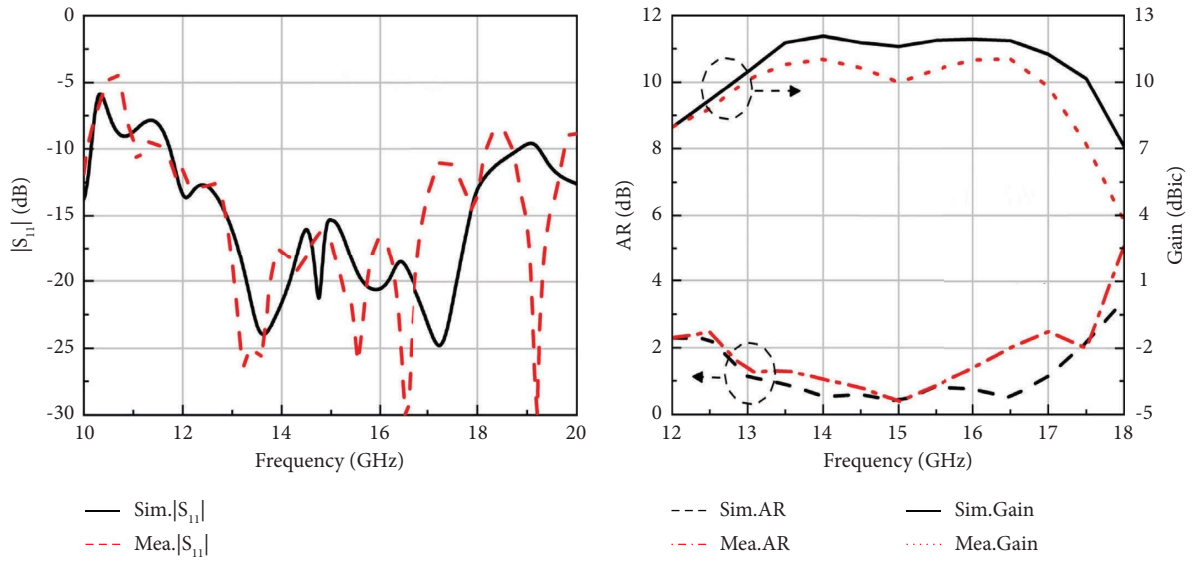

(a) (b)

Figure 11: Simulated and measured results of the proposed 2 × 2 array. (a) $|S_{11}|$. (b) 3 dB AR and gain.

12–17.8 GHz, while the simulated 3 dB gain bandwidth is 33.3% (12.5–17.5 GHz) with a peak gain of 12.06 dBic at 14 GHz, and the measured one is 34.6% (12.2–17.3 GHz) with a peak gain of 11.02 dBic at 14 GHz. The corresponding simulated and measured antenna efficiencies are about 83.9% and 66.1%, respectively. The above slight deviations between the simulated and measured results are mainly due to the following factors: (1) unexpected tolerances in the fabrication process; (2) the variation of loss tangent and dielectric constant of substrates and additional losses such as the connector loss and the impedance mismatch loss; and (3) measurement errors, such as alignment error between the measured antenna and the probe of the near-field measurement system leads to receiving loss.

Figure 12 presents the simulated and measured radiation patterns at 12 GHz, 15 GHz, and 17 GHz, respectively, as can be seen from which, they are in good agreement with each other. However, if we compare the patterns in xoz-plane and those in yoz-plane, we can see the accordance of the xoz-plane patterns between the simulated, and the measured is a little better than that in the yoz-plane. The slight discrepancy of patterns in yoz-plane is mainly caused by the metal structures on the yoz-plane, as shown in Figure 10(b), such as the L-type connector and metal frame; they have been ignored in simulations.

Furthermore, a detailed performance comparison between our work and similar works on wideband CP antenna is listed in Table 2. It is shown that our element achieves the widest impedance bandwidth of 40% with the most compact structure. Although [6, 19], respectively, achieved the largest bandwidth and the largest gain; however, the designed arrays have a highest profile. At the same time, our designed array achieves the largest CP bandwidth while with the lowest profile.

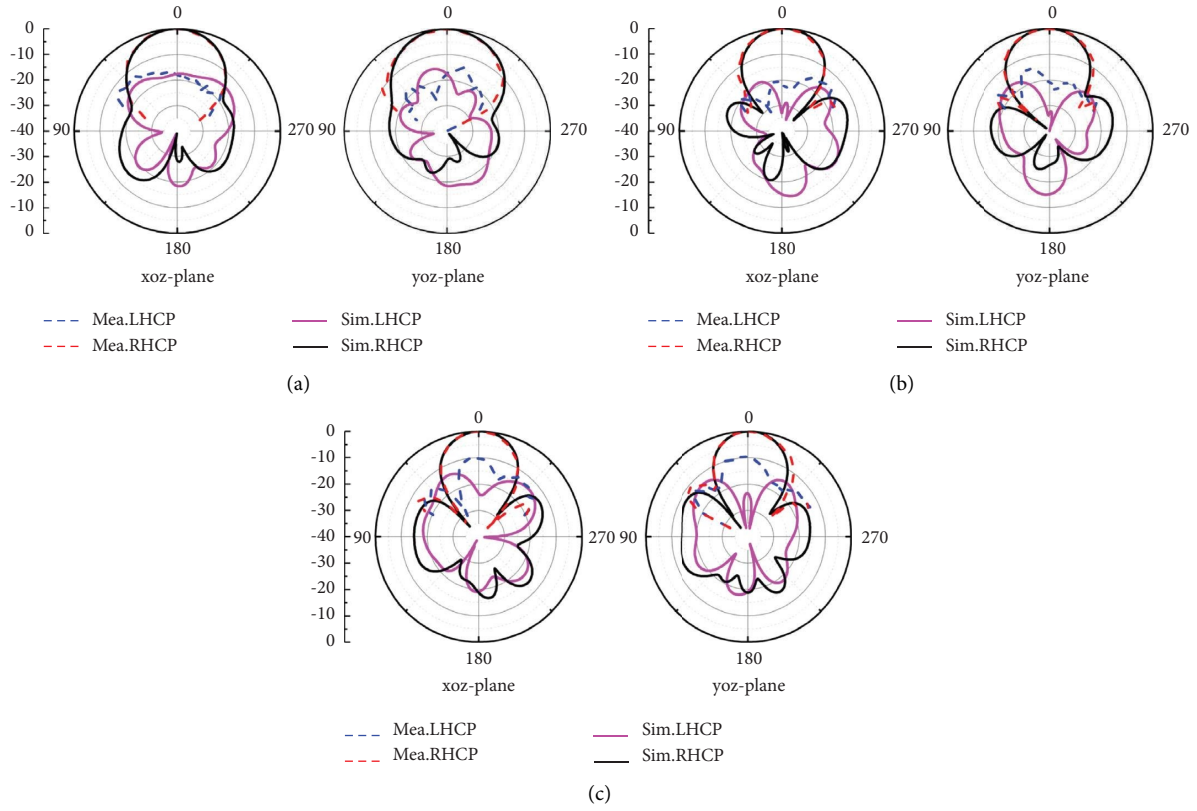

Figure 12: Simulated and measured radiation patterns of the proposed 2 × 2 array. (a) $f = 12$ GHz. (b) $f = 15$ GHz. (c) $f = 17$ GHz.

Table 2: Comparison of bandwidth and gains.

Ref	Center freq. (GHz)	Element		Array				
		Type	$\|S_{11}\|$ BW (%)	Scale	Size (λ_0^3)	$\|S_{11}\|$ BW (%)*	Peak gain (dBic)	CP BW (%)
[6]	17	Dielectric resonator with SIW excited	40	2 × 2	4.13 × 3.57 × 1.45	37.6	13.2	37
[9]	11.7	Stacked dielectric resonator	33	2 × 2	2.79 × 2.0 × 0.3	25.1	15.1	24
[13]	12.7	Stacked patches	32	4 × 4	3.0 × 3.0 × 1.4	>27.9	17	27.9
[14]	10	Cavity-backed patches	17	2 × 2	3.7 × 3.7 × 0.11	21	13.2	18
[15]	13.3	3D M-probe	22.2	2 × 2	3.0 × 3.0 × 0.14	30	11.8	28.6
[19]	13	Waveguide	21	4 × 4	3.6 × 3.6 × 3	27	22	23
This work	14.6	Heart-shaped dipole	40	2 × 2	1.89 × 1.65 × 0.11	44	11.02	34.6

* λ_0 is free-space wavelength at central frequency.

5. Conclusions

In this paper, a 2 × 2 wideband CP antenna array at Ku-band based on the proposed crossed-dipole element with a novel feeding structure has been designed, fabricated, and measured. The metal via feeding structure supports the CDE operation at high frequencies, as well as simplifies the assembly process and is easy to be integrated into the antenna because the welding is avoided. The measured results agree with the simulated results very well, which shows the CP bandwidth of 34.6% and the peak gain of 11.02 dBic, which have been achieved. The latest works on similar CP arrays have been compared showing the better performance of our design.

Data Availability

The data used to support the findings of this study are included within the article.

Conflicts of Interest

The authors declare that they have no conflicts of interest.

Acknowledgments

This work was supported in part by the National Natural Science Foundation of China (grant no. 61901451) and the Youth Innovation Promotion Association of Chinese Academy of Sciences (grant no. 2022148).

References

[1] S. S. Gao, Q. Luo, and F. Zhu, "Introduction to circularly polarized antennas," in *Circularly Polarized Antennas*, pp. 1–28, Wiley, London, UK, 2014.

[2] X. Xu, W.-Y. Yin, G. Xu, and R. Chen, "Dual-band aperture-shared circular polarized array antenna for X-/Ku-Band satellite communications," in *Proceedings of the 2020 IEEE MTT-S International Conference on Numerical Electromagnetic and Multiphysics Modeling and Optimization (NEMO)*, pp. 1–4, Hangzhou, China, December 2020.

[3] J. M. Inclan Alonso, G. Amazares Calderon, and M. Sierra Perez, "SIW antenna with polarizer at ku-band," *IEEE Transactions on Antennas and Propagation*, vol. 63, no. 6, pp. 2782–2786, 2015.

[4] C. Turkmen and M. Secmen, "Dual-band omnidirectional and circularly polarized slotted waveguide array antenna for satellite telemetry and telecommand," *IEEE Antennas and Wireless Propagation Letters*, vol. 20, no. 11, pp. 2100–2104, 2021.

[5] S. S. Gao, Q. Luo, and F. Zhu, "Circularly polarized arrays," in *Circularly Polarized Antennas*, pp. 191–261, Wiley, London, UK, 2014.

[6] Y.-X. Zhang, Y.-C. Jiao, and L. Zhang, "Wideband circularly polarized array antennas with sequential-rotation polarization grid and simplified full-SIW feeding networks," *IEEE Transactions on Antennas and Propagation*, vol. 68, no. 8, pp. 6088–6097, 2020.

[7] J. M. Kovitz and Y. Rahmat-Samii, "Using thick substrates and capacitive probe compensation to enhance the bandwidth of traditional CP patch antennas," *IEEE Transactions on Antennas and Propagation*, vol. 62, no. 10, pp. 4970–4979, 2014.

[8] Y. Liu, X. Liang, X. Zhang et al., "A K-band broadband circularly polarized slot antenna based on L-shaped waveguide cavity," *IEEE Antennas and Wireless Propagation Letters*, vol. 20, no. 9, pp. 1606–1610, 2021.

[9] W.-W. Yang, W.-J. Sun, H. Tang, and J. X. Chen, "Design of a circularly polarized dielectric resonator antenna with wide bandwidth and low axial ratio values," *IEEE Transactions on Antennas and Propagation*, vol. 67, no. 3, pp. 1963–1968, 2019.

[10] X. Q. Nasimuddin and Z. N. Chen, "A wideband circularly polarized antenna for low mutual coupling Ka-band phased arrays," in *Proceedings of the 2016 IEEE Region 10 Conference (TENCON)*, pp. 1065–1067, Singapore, November 2016.

[11] Y. H. Yang, J. L. Guo, B. H. Sun, Y. M. Cai, and G. N. Zhou, "The design of dual circularly polarized series-fed arrays," *IEEE Transactions on Antennas and Propagation*, vol. 67, no. 1, pp. 574–579, 2019.

[12] J. Huang, "A technique for an array to generate circular polarization with linearly polarized elements," *IEEE Transactions on Antennas and Propagation*, vol. 34, no. 9, pp. 1113–1124, 1986.

[13] K. M. Ibrahim, W. M. Hassan, E. A. Abdallah, and A. M. Attiya, "Wideband sequential feeding network for Ku-band dual circularly polarized 4 × 4 antenna array," *International Journal of RF and Microwave Computer-Aided Engineering*, vol. 30, no. 9, 2020.

[14] J. Zhang, Z. Xing, J. Li, D. Luo, and C. Y. D. Sim, "A low-profile ultrawideband circularly polarized slot antenna array based on artificial magnetic conductor array reflector," *International Journal of RF and Microwave Computer-Aided Engineering*, vol. 32, no. 7, 2022.

[15] H. W. Lai, D. Xue, H. Wong, K. K. So, and X. Y. Zhang, "Broadband circularly polarized patch antenna arrays with multiple-layers structure," *IEEE Antennas and Wireless Propagation Letters*, vol. 16, pp. 525–528, 2017.

[16] C. Li, X. Zhu, P. Liu, C. Yu, and W. Hong, "A metasurface-based multilayer wideband circularly polarized patch antenna array with a parallel feeding network for Q-band," *IEEE Antennas and Wireless Propagation Letters*, vol. 18, no. 6, pp. 1208–1212, 2019.

[17] S. Karamzadeh and V. Rafiei, "Modification of metasurface-based CP array antenna by using cascade feed network," *IET Microwaves, Antennas and Propagation*, vol. 13, no. 9, pp. 1334–1337, 2019.

[18] C. Ma, Z. Ma, and X. Zhang, "Millimeter-wave circularly polarized array antenna using substrate-integrated gap waveguide sequentially rotating phase feed," *IEEE Antennas and Wireless Propagation Letters*, vol. 18, no. 6, pp. 1124–1128, 2019.

[19] H. Wang, X. Lei, T. Duan et al., "A novel broadband circularly polarised waveguide slot array antenna with a wide axial ratio bandwidth," *IET Microwaves, Antennas and Propagation*, vol. 16, no. 6, pp. 359–366, 2022.

[20] A. Chen, Y. Zhang, Z. Chen, and S. Cao, "A Ka-Band High-Gain Circularly Polarized Microstrip Antenna Array," *IEEE Antennas and Wireless Propagation Letters*, vol. 9, no. 1, pp. 1115–1118, 2010.

[21] Y. Zou, H. Li, Y. Xue, and B. Sun, "A high-gain compact circularly polarized microstrip array antenna with simplified feed network," *International Journal of RF and Microwave Computer-Aided Engineering*, vol. 29, no. 12, 2019.

[22] S. X. Ta and I. Park, "Planar wideband circularly polarized metasurface-based antenna array," *Journal of Electromagnetic Waves and Applications*, vol. 30, no. 12, pp. 1620–1630, 2016.

[23] P. PourMohammadi, P. Fei, H. Nasseri et al., "A single-layer compact wideband circularly-polarized patch array for 5G communications," *IEEE Antennas and Wireless Propagation Letters*, vol. 22, pp. 1–5, 2022.

[24] Y. He, W. He, and H. Wong, "A wideband circularly polarized cross-dipole antenna," *IEEE Antennas and Wireless Propagation Letters*, vol. 13, pp. 67–70, 2014.

[25] H. H. Tran, S. X. Ta, and I. Park, "Single-feed, wideband, circularly polarized, crossed bowtie dipole antenna for global navigation satellite systems," *Journal of electromagnetic engineering and science*, vol. 14, no. 3, pp. 299–305, 2014.

[26] Y. M. Pan, W. J. Yang, S. Y. Zheng, and P. F. Hu, "Design of wideband circularly polarized antenna using coupled rotated vertical metallic plates," *IEEE Transactions on Antennas and Propagation*, vol. 66, no. 1, pp. 42–49, 2018.

[27] Y. Feng, J. Li, B. Cao, J. Liu, G. Yang, and D. J. Wei, "Cavity-backed broadband circularly polarized cross-dipole antenna," *IEEE Antennas and Wireless Propagation Letters*, vol. 18, no. 12, pp. 2681–2685, 2019.

[28] L. Zhang, S. Gao, Q. Luo, W. Li, Y. He, and Q. Li, "A wideband circularly polarized tightly coupled array," *IEEE Transactions*

on Antennas and Propagation, vol. 66, no. 11, pp. 6382–6387, 2018.

[29] S. X. Ta, I. Park, and R. W. Ziolkowski, "Crossed dipole antennas: a review," *IEEE Antennas and Propagation Magazine*, vol. 57, no. 5, pp. 107–122, 2015.

[30] G. Feng, L. Chen, X. Wang, X. Xue, and X. Shi, "Broadband circularly polarized crossed bowtie dipole antenna loaded with parasitic elements," *IEEE Antennas and Wireless Propagation Letters*, vol. 17, no. 1, pp. 114–117, 2018.

[31] W. He, Y. He, Y. Li, S. W. Wong, and L. Zhu, "A compact ultrawideband circularly polarized antenna array with shared partial patches," *IEEE Antennas and Wireless Propagation Letters*, vol. 20, no. 12, pp. 2280–2284, 2021.

[32] J. Li, Y. Hu, L. Xiang, W. Kong, and W. Hong, "Broadband circularly polarized magnetoelectric dipole antenna and array for K-band and ka-band satellite communications," *IEEE Transactions on Antennas and Propagation*, vol. 70, no. 7, pp. 5907–5912, 2022.

[33] Z. H. Zhao, L. F. Zhang, L. S. Wu, and J. F. Mao, "A cross dipole antenna array in LTCC for satellite communication," in *Proceedings of the 8th IEEE MTT-S International Wireless Symposium (IWS) part of China Microwave Week*, Nanjing, China, May 2021.

[34] D. M. Pozar, "Transmission line theory," in *Microwave Engineering*, pp. 48–94, Wiley, New York, NY, USA, 2004.

[35] L. Bian, Y. X. Guo, L. C. Ong, and X. Q. Shi, "Wideband circularly-polarized patch antenna," *IEEE Transactions on Antennas and Propagation*, vol. 54, no. 9, pp. 2682–2686, 2006.

[36] S. Y. Eom and H. K. Park, "New switched-network phase shifter with broadband characteristics," *Microwave and Optical Technology Letters*, vol. 38, no. 4, pp. 255–257, 2003.

[37] T. Bee Yen, R. Cahill, and V. F. Fusco, "Understanding and measuring circular polarization," *IEEE Transactions on Education*, vol. 46, no. 3, pp. 313–318, 2003.